Direct pore level simulation of premixed gas combustion in porous inert media using detailed chemical kinetics

Ilian Dinkov*, Peter Habisreuther, Henning Bockhorn

Karlsruhe Institute of Technology, Engler-Bunte-Institute, Division of Combustion Technology, Engler-Bunte-Ring 1, 76131 Karlsruhe, Germany

Abstract

Combustion inside of an inert ceramic matrix offers the possibility to gain high flame stability at ultra-lean conditions combined with relatively high thermal loads and low emission of pollutants. The solid matrix contributes to this behavior due to its high thermal conductivity and also high thermal inertia. Both properties lead to good stabilization and homogenization of the reaction zone. As the experimental access, optical as well as with probes, is inherently limited due to the solid structure, numerical examination of the reacting flow field is done via 3D direct solution of the momentum, energy and species balance equations without further modeling assumption for the solution of the flow field (direct pore level simulation, DPLS). The Kee reaction mechanism including 17 species and 58 reactions is integrated in the solver for the calculation of the species conversion. The results of the 3D DPLS are compared with experimental data of a cylindrical, axial-flow porous burner and show good agreement with respect to temperature and macroscopic flame thickness. The DPLS results showed that the flame structure is substantially affected by the topology of the PIM at the pore level.

Introduction

Premixed combustion in porous inert media (PIM) in comparison with free laminar flames features considerably higher burning rates, less pollutant emissions, higher radiant heating rates and increased heat recirculation due to solid-solid radiation, solid conduction and dispersion. The above mentioned advantages strongly advocate the use of porous burners as a potential alternative to conventional free flame burners (2; 8).

The increased local reaction rate of combustion in PIM, leads to extension of the lean stability limit and to higher area specific loads. Therefore it is possible to increase the input power, to burn lean mixtures or low grade fuels and to generate directly the products at a temperature acceptable to machinery downstream. Additionally, due to the solid material properties, high rates of thermal radiation are emitted, thus it is meaningful to use this kind of burners for industrial processes utilizing radiant heating (5; 9; 8; 11).

State of the art studies about combustion in PIM (11; 7) indicate that the enhanced combustion in PIM, is due to coupled heat recirculation and hydrodynamic dispersion (3), as shown in Fig.1. After ignition, a considerable amount of enthalpy from the hot burned gas is transported by convection to the solid matrix. Since the thermal transport properties of solid matter are around two orders of magnitude higher than those of gas at atmospheric conditions, the heat is transferred upstream by conduction and solid-solid radiation through the PIM. At the burner inlet, the solid temperature is higher than the unburned gas mixture, so a convective heat flow from the solid is established. Thus a preheating of the incoming gas mixture is possible, without dilution with recirculated burned gases.

*Corresponding author: ilian.dinkov@kit.edu

Proceedings of the European Combustion Meeting 2015

In addition, there is a preheating due to dispersion, which enhances both mass and heat transport in the gas phase, due to transverse mixing along tortuous flow paths imposed by the random geometry of porous media. Thus the effective coefficient of dispersion is around two orders of magnitude higher than the molecular diffusivity at atmospheric conditions of both, species and heat. It augments substantially the species transport and the macroscopic heating rate of incoming unburned gas, in comparison to an empty pipe flow.

Due to these two phenomena, the heat release rate i.e. the burning rate S and the flame thickness are increased according to the effective transport properties of PIM.

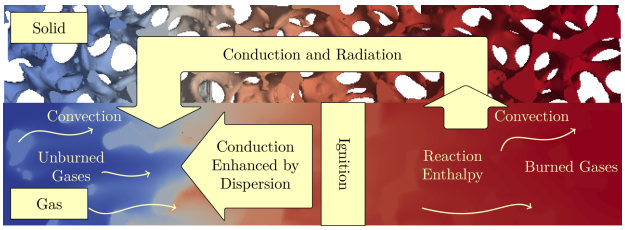

Figure 1: Sketch of coupling heat transport mechanisms in PIM.

Specific Objectives

The objective of the performed DPLS is to employ a commercially available CFD code with its standard discretization methods for the prediction of the complex mixing and reaction field in a real porous structure obtained from computer tomography, to gain detailed information about the processes occurring at both macroscopic and pore level. Additionally, the rate of simplification of different reaction kinetics is numerically investigated, in order to make obvious their influence on the temperature

field and the position of the macroscopic flame front during the combustion inside the porous structure.

Numerical setup DPLS

The software ANSYS CFX 15 was used for modeling premixed combustion of CH_4 and air. The Finite Rate Chemistry model was applied for all investigated reachtion mechanisms. This laminar model computes the chemical source terms (rate of species conversion) using temperature and pressure dependent rate coefficients of the individual reactions. The numerical calculations were carried out using three different levels of simplification of the reaction kinetics:

- Single step, global reaction mechanism by Westbrook and Dryer with *5 Species and 1 Reaction* - WD1-Set3 (10)
- Two step reaction mechanism (incl. CO-formation and oxidation) by Westbrook and Dryer with *6 Species and 2 Reactions* - WD2-Set3 (10)
- Detailed reaction mechanism (Kee) with *17 Species and 58 Reactions*- Kee (6)

The reactions included in the two global mechanisms are shown in Tab.1.

Single step mechanism	Two step mechanism	Detailed reaction mechanism (Kee)
$CH_4 + 2O_2 = CO_2 + 2H_2O$	$CH_4 + 3/2O_2 = CO + 2H_2O$ $CO + 1/2O_2 = CO_2$	58 Reactions

Table 1: Reachtion mechanisms for the DPLS calculations

Computational grid

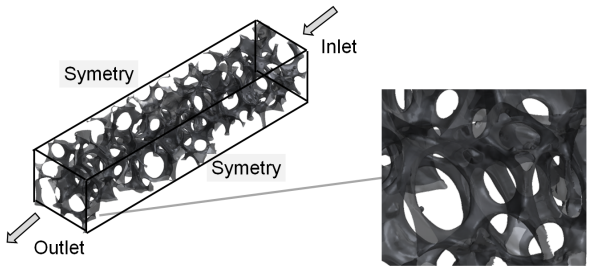

Figure 2: Computational domain / Surface of the solid domain for DPLS of a segment of the cylindrical, axial-flow porous burner

Starting point for the generation of the computational grid comprising two domains representing the solid part of the PIM and the fluid domain are the 3D images of the sponges (reticulated PIM structure of SiSiC, 10 PPI, 87% porosity), acquired by μ-CT and consisting of gray values for 3072 x 1024 x 1024 voxels of the investigated SiSiC sponge sample. Details of the PIM structure and

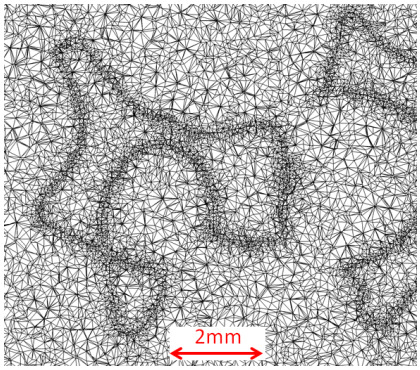

Figure 3: Part of the computational grid

of the technique for acquiring this data are given in (4). Using the 3D volume data of the sponge, a model of the interface from solid to fluid could be extracted with digital filter routines for noise reduction and a threshold value to separate solid from void.

The whole procedure yields the discretized interface comprising 5 million connected triangles. In order to construct the 3D computational grid from this surface a standard meshing tool (ANSYS ICEM CFD) was used. Fig.2 shows the computational domain for the DPLS, which represents a segment of the cylindrical, axial flow porous burner investigated experimentally. The numerical domain is 45 mm long and has a 9x9 mm^2 cross section at inlet and outlet area. The resulting numerical grid was locally refined near the solid phase walls. It comprised approx. 7 Mio. elements for the fluid part (1.5 Mio. nodes) and 3 Mio. elements for the solid part (1 Mio. nodes). Figure 3 shows a cut through a part of the computational grid including fluid, solid part and the refinement near the solid walls.

Boundary conditions and property data

The flow field during the combustion in PIM can be presumed as laminar (stationary, without fluctuations in time). The averaged Re - Number, defined with the averaged pore diameter of approx. $6.5mm$ as a specific length, has values in the preheating zone and in the area of the macroscopic flame front between 103 and 200 for the investigated air equivalence ratios (fully turbulent flow ($Re_{Dpore} > 300$). Therefore no turbulence modeling is necessary for the calculations. Additionally the average spatial resolution of the num. grid was 50 $points/mm^3$, i.e. 6 $points/mm$ including the refinement near the walls. By using the pore diameter of approx. 6.5 mm as a specific length scale for the flow field, the grid density of the DPLS is approx. 26 $points/pore$. When using this, the simulation could be regarded as a direct numerical simulation concerning the flow field in the PIM.

The model intrinsically includes the interaction between the fluid and the solid material: heat convection between phases, conduction through the solid and the influence of the flow dispersion. For the calculations, surface (catalytic) reactions on the solid material are neglected.

Fig.2 depicts the boundary conditions used for the calculations. The mass flow rate value was set for the simulation. It was adjusted until the resulting flame stabilized in the computational domain.

Results and Discussion

In order to give an overview over the local distribution and spatial inhomogeneity of velocity and temperature, Fig.4 presents the local axial velocity and temperature distribution in gas and solid phases obtained by the DPLS along the middle annular plane parallel to the flow direction using the detailed reaction mechanism including 17 Species and 58 Reactions.

The detailed information of the combustion in PIM obtained from the DPLS clearly shows the randomness of the process on pore level and can be roughly described as preheating of unburned mixture from the solid surfaces of PIM, from where the heat is transferred to regions of the gas with higher velocity like the center of the pore due to tortuous mixing (dispersion). Additionally, the mixture is ignited at the solid surface, but also due to dispersion, it is quenched in the regions with faster gas flow increasing its temperature, before it collides against an other wall where the reaction can continue. Due to the randomness of the porous structure, the flow in PIM is accelerated in the pores and decelerated near the solid structure walls. This leads to considerably high velocity variations, especially in the region of the macroscopic flame front after the ignition, where the maximum velocity gradient is located.

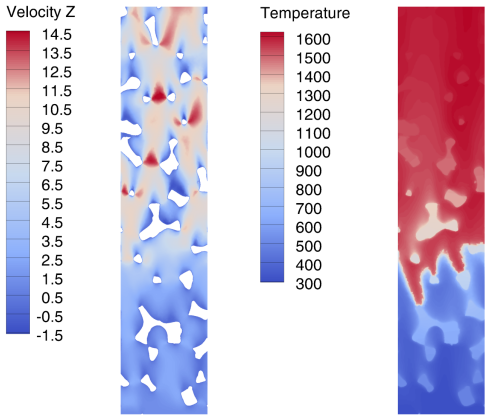

Figure 4: Local axial velocity (left) and temperature (right) distribution along the middle annular plane of PIM - DPLS, Kee, λ=1.6, T_0=300K, p=1bar.

Figure 5 shows the local OH mass fraction (left) and H_2O mass fraction (right) distribution along the middle annular plane of PIM predicted by the detailed reaction mechanism. The OH mass fraction depicts the position of the flame front during the combustion process. With respect to the OH and the temperature distribution, it certainly can be observed that the position of the macroscopic flame front in PIM takes a longitudinal region thicker than $8mm$, which is considerably wider than the flame thickness of a laminar premixed flame ($2mm$). This result also corresponds with the increased values of the burning velocity in PIM observed in different studies (2; 1; 8). This thickenning of the flame front leads to a wider species conversion region as depicted by the CO_2 mass fraction distribution in Figure 6 - right. The wider region for conversion, also of the intermediate species such as CO, is obvious on the left side of figure 6 where the CO mass fraction distribution along the middle annular plane of PIM is shown. The maximum values of the CO mass fraction corresponds with this of the OH mass fraction and the position of the flame front. CO is build in the main reaction region and then is oxidated to CO_2 in the reburn zone.

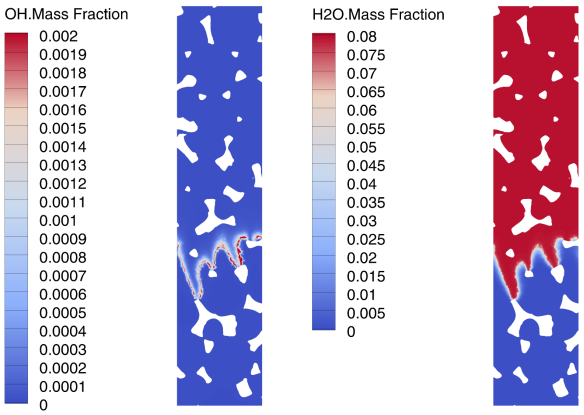

Figure 5: Local OH mass fraction (left) and H_2O mass fraction (right) distribution along the middle annular plane of PIM - DPLS, Kee, λ=1.6, T_0=300K, p=1bar.

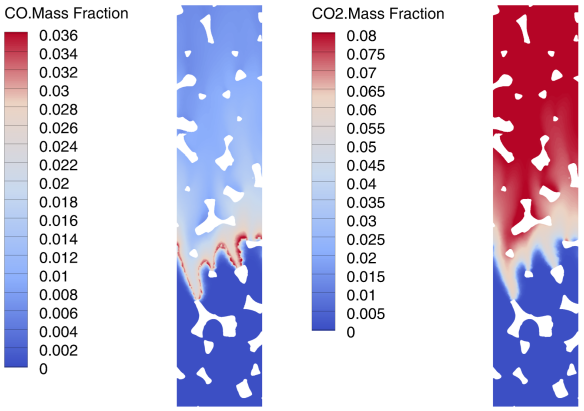

Figure 6: Local CO mass fraction (left) and CO_2 mass fraction (right) distribution along the middle annular plane of PIM - DPLS, Kee, λ=1.6, T_0=300K, p=1bar.

Figure 7 depicts the gas and solid temperature distribution and also the conversion of the combustion reactants and important intermediate species as averaged values along the PIM. The gas temperature and the species

mass fractions reported from the DPLS results represents mass flow averaged values along the cross sectional area. While the solid temperature reported is area averaged also along the cross section. For that, the domain was discretized at around 5 planes/mm in the macroscopic flow direction. It can be clearly observed that the fuel - CH_4 is completely oxidized and the values of the combustion products are at the end of domain constant.

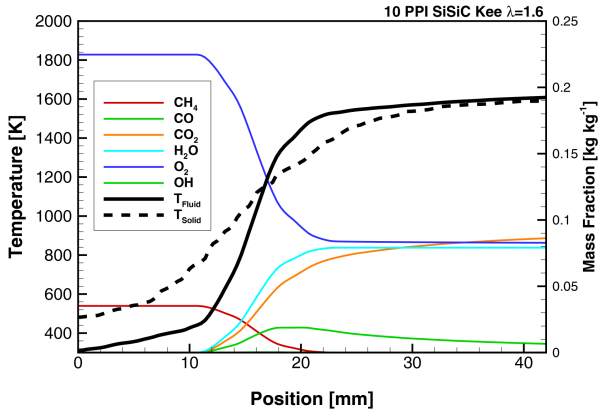

Figure 7: Averaged fluid and solid temperature and species mass fraction distribution along PIM - DPLS, Kee, λ=1.6, T_0=300K, p=1bar.

Figure 8 shows the temperature distribution along the middle annular plane of the numerical domain, predicted with the detailed reaction mechanism and the both reduced mechanisms - the two step reaction mechanism (WD2) and the single step, global reaction mechanism (WD1) at the same inlet boundary conditions, i.e. mass-flow rate and air to fuel ratio. Comparing the three reaction mechanisms applied in the numerical calculations at λ=1.6 and T_0=300K, the most remarkable differences are the global temperatures and the position of the macroscopic flame front. The both, single step and the two step reaction mechanisms overestimated the measured temperature due to neglecting of dissociation reactions, which also leads to higher burning rates. Due to this higher burning rates, it can be observed that the predicted flame position is moved upstream in the calculations with the two step (WD2) and the single step, global reaction mechanism (WD1).

This upstream shifted flame front is also illustrated in Figure 9 where the temperatures, predicted by DPLS with the three different reaction mechanisms, are compared with experimental data from a cylindrical, axial-flow porous burner at λ=1.6 (2). The comparison between DPLS and experimental data shows the ability of the DPLS, especially using the detailed reaction mechanism to reproduce the temperature gradient and the macroscopic flame thickness in the experiments. The temperature gradient obtained by the measurements exhibits values between the calculated gas and solid phase temperatures, which indicates the influence of the solid phase

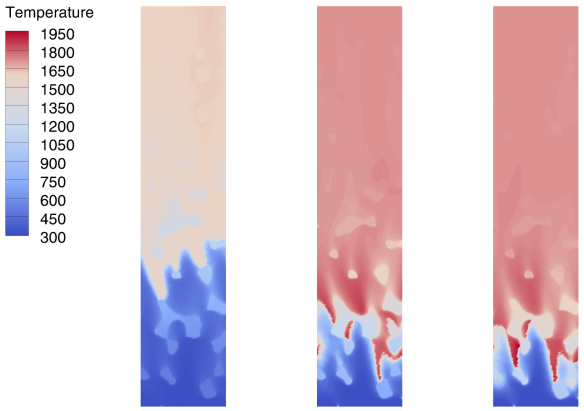

Figure 8: Temperature distribution along the middle annular plane of PIM calculated with different reaction mechanisms - detailed - Kee (left), two step - WD2 (center) and single step - WD1 (right) at λ=1.6, T_0=300K, p=1bar.

radiation. The maximum temperatures are slightly underestimated by the detailed reaction mechanism.

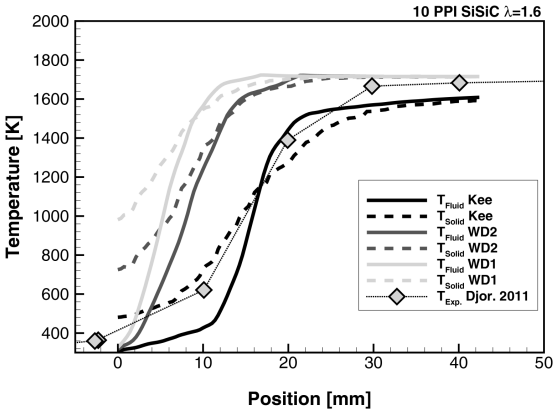

Figure 9: Comparison of the averaged fluid and solid temperature distribution along PIM obtained with the different reaction mechanisms and experimental data from (2).

Conclusions

In this study direct pore level simulations (DPLS) were performed on a 3D computational grid consisting of the solid and fluid domains. The calculations were performed in a real porous inert structure obtained from computer tomography (reticulated PIM structure of SiSiC, 10PPI, 87% porosity). A detailed reaction mechanism including 17 species and 58 reactions is integrated into the solver for the calculation of the species conversion. The calculation of the chemical source terms (rate of species production) was carried out using temperature and pressure dependent rate coefficients of the individual reactions. The rate of simplification of different reaction ki-

netics are numerically investigated. The comparison of the temperature profiles leads to the conclusion, that the detailed reaction mechanism is predicting the temperature rise and the thickening of the flame front more accurate then the single (WD1) and the two step (WD2) reaction mechanism. The results of the DPLS are compared with experimental data of a cylindrical, axial-flow porous burner and show good agreement with respect to temperature and macroscopic flame thickness. The DPLS results showed that the flame structure is substantially affected by the topology of the PIM at the pore level. The flame is anchored at solid struts and spans downstream in regions with higher velocity. Thus the detailed flame structure is corrugated and discontinuous, although it does not change along time. Therefore, considerable lateral variations of parameters such as temperatures, velocity and concentrations are present along the space. These spatial fluctuations in the region of the macroscopic flame front represents the three-dimensionality of the flame inside the PIM and need to be considered by the 1D calculations while calculating species and conversion rate.

References

[1] BARRA, A. ; ELLZEY, J.: Heat recirculation and heat transfer in porous burners. In: *Combustion and Flame* 137 (2004), Nr. 1-2, S. 230 – 241

[2] DJORDJEVIC, N.: *Flammenstabilisierung durch Verbrennung in festen Schwaemmen*, Karlsruhe Institute of Technology, Karlsruhe, Germany, Diss., 2011

[3] DJORDJEVIC, N. ; HABISREUTHER, P. ; ZARZALIS, N.: Experimental study on the basic phenomena of flame stabilization in a porous burner for a premixed combustion application. In: *Energy Fuels* 26 (2012), S. 6705–6719

[4] GROSSE, J. ; DIETRICH, B. ; GARRIDO, Gerardo I. ; HABISREUTHER, P. ; ZARZALIS, N. ; MARTIN, H. ; KIND, M. ; KRAUSHAAR-CZARNETZKI, B.: Morphological Characterization of Ceramic Sponges for Applications in Chemical Engineering. In: *Industrial & Engineering Chemistry Research* 48 (2009), S. 10395–10401

[5] HOWELL, J. R. ; HALL, M. J. ; ELLZEY, J. L.: Combustion of hydrocarbon fuels within porous inert media. In: *Progress in Energy and Combustion Science* 22 (1996), S. 121–145

[6] KEE, J. ; RUPLEY, F. ; MILLER, J.: Chemkin-II: A Fortran chemical kinetics package for the analysis of gas-phase chemical kinetics / Report No. SAND89-8009B, Sandia National Laboratories. 1989.

[7] MUJEEBU, M. A. ; ABDULLAH, M. Z. ; MOHAMAD, A.A. ; BAKAR, M.Z. A.: Trends in modeling of porous media combustion. In: *Prog Energ Combust* 36 (2010), Nr. 6, S. 627 – 650. – ISSN 0360–1285

[8] TRIMIS, D. ; DURST, F.: Combustion in a Porous Medium-Advances and Applications. In: *Combustion Science and Technology* 121 (1996), Nr. 1-6, S. 153–168

[9] WEINBERG, F. J.: Combustion Temperatures: The Future? In: *Nature* 233 (1971), S. 239–241

[10] WESTBROOK, CHARLES K. ; DRYER, FREDERICK L.: Simplified Reaction Mechanisms for the Oxidation of Hydrocarbon Fuels in Flames. In: *Combustion Science and Technology* 27 (1981), Nr. 1-2, S. 31–43

[11] WOOD, Susie ; HARRIS, Andrew T.: Porous burners for lean-burn applications. In: *Prog Energ Combust* 34 (2008), Nr. 5, S. 667 – 684. – ISSN 0360–1285